IEEE Access
Multidisciplinary ⋮ Rapid Review ⋮ Open Access Journal

Received 16 November 2024, accepted 12 December 2024, date of publication 18 December 2024,
date of current version 30 December 2024.

Digital Object Identifier 10.1109/ACCESS.2024.3519699

RESEARCH ARTICLE

Decoding EEG Signals During the Observation of Robotic Arm Movements

PIETRO CIMAROSTO[1], KYRIAKI KOSTOGLOU[2], LUCA TONIN[1], (Senior Member, IEEE), AND GERNOT MÜLLER-PUTZ[2,3], (Senior Member, IEEE)

[1]Intelligent Autonomous System Laboratory, Department of Information Engineering (DEI), University of Padova, 35129 Padua, Italy
[2]Institute of Neural Engineering, Graz University of Technology, 8010 Graz, Austria
[3]BioTechMed-Graz, 8010 Graz, Austria

Corresponding author: Gernot Müller-Putz (gernot.mueller@tugraz.at)

This work was supported by the TU Graz Open Access Publishing Fund.

This work involved human subjects or animals in its research. Approval of all ethical and experimental procedures and protocols was granted by the Ethics Committee of the Medical University of Graz.

ABSTRACT Recent studies in the domain of invasive brain-computer interfaces (BCIs) have revealed that neural activity recorded during the observation of robotic movements in a reach-and-grasp task carries information that can be utilized to improve the active online decoding of motor intention. In the non-invasive domain, the spectral characteristics of human brain activity during the observation of robotic movements has been widely investigated. However, focusing only on the frequency components of electroencephalography (EEG) for motor control decoding is a poorly suitable strategy due to its scarce temporal resolution. Following a different approach, we explored temporal features of EEG filtered in the delta band (Low-Frequency EEG, or LF-EEG) for the continuous decoding of control-oriented kinematic trajectories. We designed an experimental paradigm aimed at investigating how the observation of center-out target-oriented reaching movements executed by a robotic arm in the 2D plane is encoded in low-frequency EEG signals. By employing machine learning algorithms and novel approaches, we were able to continuously decode the LF-EEG into movement trajectories, achieving performance significantly above chance-level. This confirms that low-frequency neural activity measured non-invasively during a movement observation task contains adequate amounts of movement-related information for BCI applications.

INDEX TERMS Brain-computer interfaces, electroencephalography, robotic arm, movement observation, observation-based calibration.

I. INTRODUCTION

In recent years, brain-computer interfaces (BCIs) represent a rapidly developing field of research, as they allow the translation of an individual's intentions into artificial outputs and interactions with the external environment [1]. The primary objective of BCIs is to circumvent the natural output of the brain, and possibly restore it in the case of users with disabilities. Focusing specifically on motor-related non-invasive BCIs, the goal is to decipher the intention of a motor action from neural signals measured at the scalp level, often through electroencephalography (EEG) which represents an efficient, portable and reliable non-invasive brain measurement technique. The main approaches for decoding neural activity through BCIs include the utilization of either spontaneous EEG and sensory-motor rhythms [2], [3], [4], [5] or event-related potentials (ERP) [2], [6], [7], [8]. These strategies are often combined with Motor Execution (ME), Motor Attempt (MA) or Motor Imagery (MI) tasks [2], [9], enabling users to select a specific goal within a discrete set of options by detecting upcoming events from their neural signals. Another approach involves the continuous decoding of kinematics from neural activity, in order to translate the neural representation of an intention into continuous commands for achieving a goal. This is particularly useful when controlling for example artificial limbs and, in general, robotic devices. Non-invasive decoding strategies

The associate editor coordinating the review of this manuscript and approving it for publication was Loris Belcastro.

involve the use of spectral features as well as event-related desynchronization and synchronisation (ERD/S) patterns in the alpha and beta bands [10], [11], [12]. To increase decoding performance, several studies have employed a process known as observation-based calibration [13], [14], [15], [16], in which the user's brain activity is recorded while passively observing a robotic upper limb performing a motor task. The obtained data are then used to build an initial version of the decoder model, which is then fine-tuned during the gradual introduction to the full closed-loop neural control of the robotic device within the same motor task. This approach was adopted in Clanton [13] and Collinger et al. [14], where the activity of the brain's cortex was recorded invasively and the neuronal firing rates were translated into robot velocities, first in primates [13] and then in a tetraplegic human [14], with promising results. The neural activity induced by the ''passive'' movement observation (MO) task and ''active'' ME or other related motor tasks exhibit distinct EEG patterns that can be utilized in the development of a decoding model through non-invasive observational data. Specifically, it was shown that the observation of motor actions in human subjects is linked to the activation of the human mirror neuron system, an ensemble of neuronal structures that is well-known in the field of invasive motor BCI [17], [18]. Its activation translates in the non-invasive domain as the phenomenon of the *mu-suppression*—i.e., the reduction of EEG power in the mu band—corresponding to the frequency range between 8 and 12 Hz (the α band), within the sensorimotor cortex [19], [20], [21]. Other effects induced by upper-limb MO tasks include the desynchronization of neural ensembles in the sensorimotor regions in the β band (12-30 Hz) and in the parieto-occipital regions in the α band [22]. These behaviours may depend on the characteristics of the movement, namely the viewpoint of the observer, the appearance of the effector (for instance, if human or robotic), and the speed of the action [17], [19], [20], [23]. However, when compared to the active execution or imagination of movement, such behaviour is to be attributed to distinct but yet interconnected processes occurring in the human brain, characterized by varying levels of activation [24], [25], [26], [27].

While EEG-based spectral features are one strategy for MO decoding, another potential approach involves extracting motor-related information from the lowest frequency range of the EEG—i.e., delta (between 0.2 Hz and 5Hz), namely, low frequency (LF) EEG (LF-EEG). Studies have demonstrated that LF-EEG inherently encodes upper-limb movement direction during motor tasks [1], [18], [28], [29], [30], [31], [32], and it can further be used to extract movement-related cortical potentials (MRCP) for the detection of self-paced movement intention [33], [34]. Despite its potential, there is limited literature exploring the use of this type of features for MO decoding. This study was developed with the objective of addressing this gap in literature by defining two research objectives: firstly, to investigate the neurophysiological effects induced by the observation of upper-limb robotic movements, with a specific focus on the more well-defined target-oriented center-out tasks. Secondly, to develop a decoder able to reconstruct offline the robotic arm's kinematic trajectories (in terms of 2D position and velocity) from the LF-EEG recorded during the observation of motor actions. In such a way, we aim to prove the feasibility of building a decoder model for kinematic control using only temporal features of delta-band filtered observational EEG data.

II. MATERIALS AND METHODS

Fifteen healthy individuals (eight females) took part in the experiment, with an average age of 22.9 $\pm$ 3.7 years, except for one outlier aged 56. All participants were right-handed and had normal or corrected-to-normal vision. All participants gave their written informed consent to take part in the study, and the experimental procedure conformed to the Declaration of Helsinki and was approved by the ethics committee of the Medical University of Graz.

In the experiment, the participant was seated in front of a screen that displayed the visual paradigm. A JACO robotic arm (Kinova Robotics, 7 controllable degrees of freedom) was placed between the screen and the participant, allowing for an egocentric viewpoint with respect to the robotic arm. Neural activity was recorded using 60 gel-based active EEG electrodes (actiCAP Brain Products GmbH, Germany) placed on the scalp according to the international 10-10 electrode system. The reference and ground electrodes were placed at the right mastoid and AFz, respectively. Four additional active electrodes were positioned at the inferior, superior and outer canthi of the left eye and to the outer canthi of the right eye to record the electro-oculographic signals (EOG). Electrodes 54 and 55 were placed in the parieto-central region to increase the spatial resolution in this area of interest, symmetrically in both hemispheres with respect to the midline, one (CPP1h) at the midpoint of CPz, CP1, Pz and P1, the other (CPP2h) at the midpoint of CPz, CP2, Pz and P2. The EEG and EOG signals were recorded at a sampling rate of 200 Hz through biosignal amplifiers (BrainAmp, Brain Products GmbH, Germany). The custom scripts for the paradigm, and the pre-processing and decoding phases were developed in Matlab (Mathworks Inc. USA, mainly Versions 2019b and 2022b). Psychotoolbox for Matlab was employed to present the stimuli. The data were recorded and synchronized through the lab streaming layer[1] (LSL) protocol, implemented in Matlab.

A. PARADIGM

The experimental sessions included an initial setup phase during which the participant was placed in the workstation wearing the EEG system and was instructed on the upcoming task, which marked the beginning of the recording session. The recording session lasted, on average, two hours. At the beginning of the session, the participants had the opportunity to review and familiarize themselves with the paradigm. Each session included a total of 15 runs. At the end of each run,

[1] https://github.com/labstreaminglayer/liblsl-Matlab

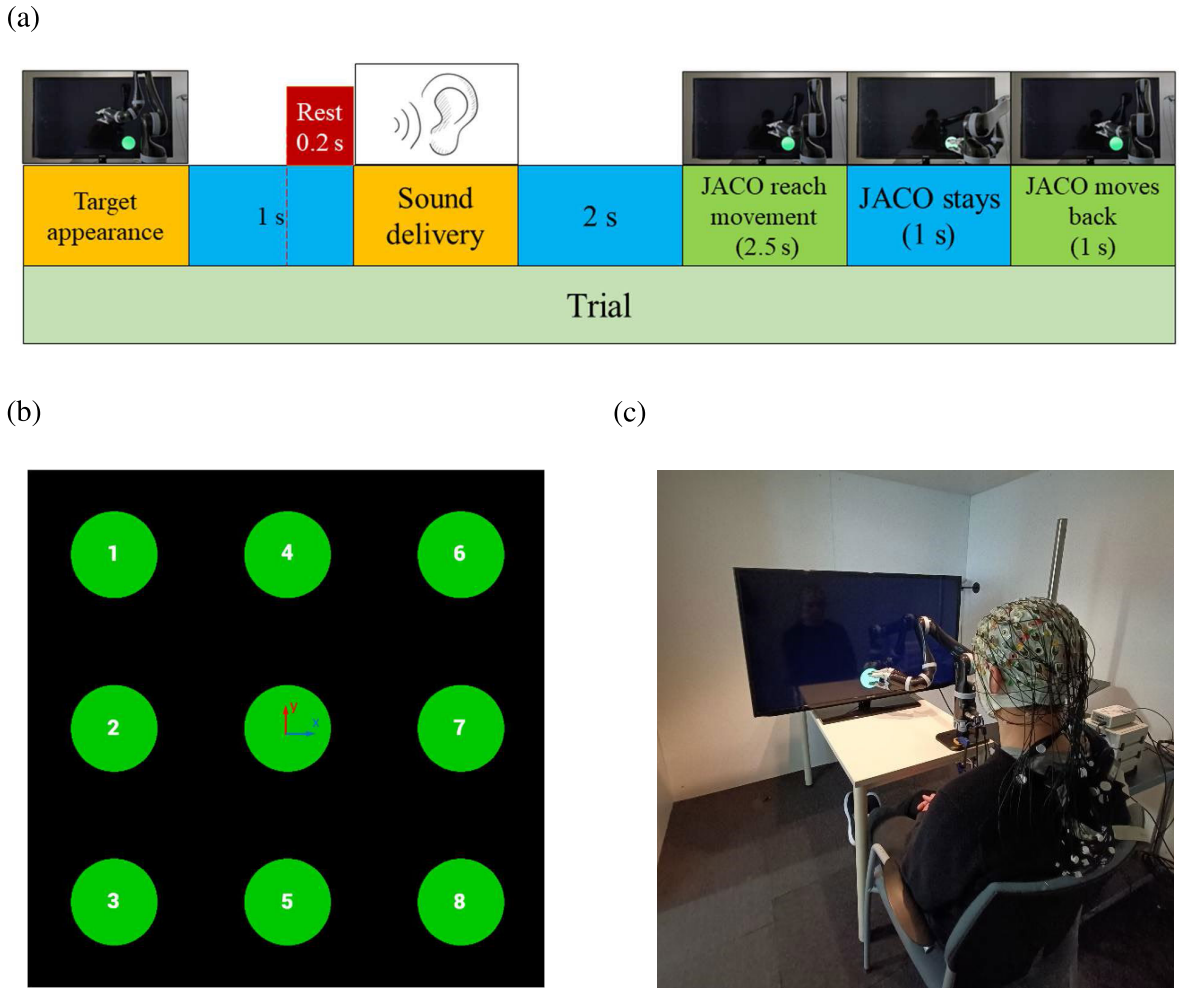

FIGURE 1. (a) Organization of phases within a *robot run* trial; (b) Enumeration of paradigm targets as displayed on the screen. (c) Experimental setup during a measurement session.

participants had the option to rest for up to 2 minutes. Midway through the recording session, after the 7th run, participants were allowed to exit the workstation freely for a maximum of 10 minutes.

The experimental paradigm included the so-called 'robot run' blocks, each consisting of 24 trials structured as depicted in Figure 1(a): for each trial, the target was randomly selected from the eight boxes within a 3×3 grid, excluding the central box, and then displayed on the screen. The participants were instructed to look at the target and acknowledge its position. An auditory stimulus was then delivered, signaling the participants to observe and track the robotic hand. At that point, the hand initially moved from its central starting position toward the target along a linear center-out path, remained at the target for one second, and then returned to its home position.

The 'eye run' blocks were designed based on the work of Kobler et al. [35], [36], Mondini et al. [37] and Pulferer et al. [9], [30] with the purpose of identifying and attenuating the effect of blinks and saccades on the EEG. The visual paradigm included four types of oculomotor tasks selected in a pseudo-random manner (rest/stare, blinks, horizontal saccades, vertical saccades). The EEG collected from the participants during the eye runs was used to build a model capable of detecting and reducing the impact of oculomotor artifacts on the robot runs data. This model was estimated using the sparse generalized eye artifact subspace subtraction algorithm (SGEYESUB) described in [35].

During a recording session, each participant underwent three eye run blocks and 12 robot run blocks (one eye run block precedes six consecutive robot run blocks, plus one eye run block before the end of the session), resulting in a total of 288 robot run trials and 57 eye run trials.

B. DATA PROCESSING

The data consisted of EEG samples collected at 200 Hz, aligned with the up-sampled horizontal and vertical position of the robotic hand during a trial, as well as the markers related to the different phases of a block. The EEG was high-pass filtered at 0.2 Hz using a first-order non-causal infinite impulse response (IIR) filter, based on the processing pipeline presented in [9], [37]. Notch filtering was employed to eliminate power-line noise interference at 50 Hz.

If channels were deemed as ''noisy'' during the experimental sessions, they were corrected afterwards by performing channel interpolation. This process involved substituting the data of such channels with the weighted sum of their four closest neighbouring channels, with the weights determined based on the inverse distance. On average, 1.1 ± 1.6 channels were interpolated for each subject, typically involving channels T7 and T8. Removal of eye artifacts was carried out based on the eye artifact correction SGEYESUB model extracted from the eye runs. Pops and drifts were removed by means of the HEAR algorithm [38], followed by the removal of EOG and AF channels and common average reference (CAR) spatial filtering.

We employed two types of analysis. In the first analysis, we decoded the observed continuous 2D position and velocity of the robotic hand using the LF-EEG signal. In the second analysis we investigated the ERD/S patterns that arise during the observation of the robotic arm movement [39]. The EEG was filtered in two different ways depending on the final purpose of the analysis: for ERD/S analysis we low-pass filtered the data using a fifth-order Butterworth low-pass filter with a cut-off frequency of 40Hz, whereas for continuous decoding, we downsampled the data to 10 Hz and applied finite impulse response (FIR) anti-aliasing low-pass filter at 5 Hz, resulting in the delta band LF-EEG signal. The computation of 2D robot velocities was performed by means of a third-order polynomial Savitzky-Golay filter (51 taps) applied on the position trajectories. The data were then epoched from 4 s before to 2.5 s after the arrival of the hand to the target. Trials were automatically rejected if either the EEG in any channel exceeded a threshold of $\pm 100 \mu V$, or exhibited abnormal probability or kurtosis (i.e., more than five standard deviations from the mean) [37], resulting in an average rejection rate of 20.5% (mean $\pm$ std: 55.43 ± 18.56) trials per participant. ERD/S maps were estimated along the time interval between 7 s before to 2.5 s after the arrival of the robotic arm to the target, using as reference period the 0.2s interval before the delivery of the auditory stimulus.

C. DECODING

Our main objective was to decode at each time point the observed continuous robotic movement (in terms of bi-dimensional position and velocity), based on the current and past LF-EEG samples within a trial. In matrix form, this can be formalized as follows,

$$f_R : X \rightarrow Y \quad with \quad X \in \mathbb{R}^{N \times T \times Tr}, Y \in \mathbb{R}^{M \times T \times Tr} \qquad (1)$$

where X is the LF-EEG, Y are the movement parameters, namely x position, y position, x velocity and y velocity relative to the hand of JACO in the 2D plane during a trial, $N = 55$ is the number of EEG channels excluding EOG and AF electrodes, T is the constant number of LF-EEG time samples of a subject's robot run trial, $M = 4$ is the number of parameters, i.e., the dimension of the kinematic state of the robotic hand's trajectory (i.e., x-position: PosX, y-position: PosY, x-velocity: VelX, y-velocity: VelY), Tr is the number of all robot run trials of a subject.

In order to capture the relationship between LF-EEG and movement, we experimented with three types of models: the partial least squares based unscented Kalman filtering (PLSUKF), the partial least squares-based support vector machines (PLSSVM) and the partial least squares-based regression tree ensembles (PLSRTE). The architecture of the models and their dataflow are further illustrated in Figure 2.

The PLSUKF is considered one of the state-of-the-art algorithms for the continuous decoding of robotic movements from the LF-EEG, often outperforming more complex algorithms despite its lightweight architecture [9], [31], [37], [40], [41]. Its design is based on two key components: a transformer component and a decoding component. The first component regresses the movement parameters — i.e., the continuous kinematic state of the robotic hand, from the LF-EEG using the PLS technique whereas reducing EEG collinearity. In fact, the PLS regression algorithm works by mapping strongly collinear predictor variables into a latent space of lower dimensionality. Here, we take advantage of this technique to reduce the dimensionality of the predictor data, i.e., the multi-lag EEG data and increase computation speed. The LF-EEG PLS latent space projection is then fed to the second component for the kinematic state (e.g., horizontal and vertical position and velocity) decoding through unscented Kalman filtering (UKF). The purpose of the UKF is to track the time evolution of the movement parameters and enhance their estimation. In contrast to the conventional Kalman filter, UKF is able to capture non-linear relationships between directional and nondirectional movement parameters, boosting prediction accuracies. The input is the matrix of the 6-samples-lagged LF-EEG (similarly to [37]), i.e., the current LF-EEG sample together with 6 past samples, corresponding to the past 0.6 seconds. The input matrix of dimensionality $D = 7\ samples \times 55\ channels = 385$ is mapped by the PLS into a subspace of dimensionality $D_{latent} = 85$, number of latent components that explains 99% of the variance in the multi-lag EEG [37]. The mapping was obtained by training the PLS regression model on the available data and by specifying the dimension of the latent space. Then, the UKF component iteratively computed the previous state's parameters and updated the complete kinematic state by incorporating information from the previous state and the latent-space projected LF-EEG. Initial parameters of the UKF were estimated at the beginning of the trial ($t = 0$) from the trial data covariance matrices, according to Mondini et al. [37]. This technique, along with other KF-based approaches, predict future states from the current state in a recursive manner. This recursive process has made them the standard for accurately predicting continuous and smooth state-space trajectories [42]. The PLSUKF algorithm is described in more detail in [37], [40]. As alternatives to the KF-based approach, two novel approaches were implemented for the decoding task. The PLSSVM model, which was designed in a similar manner as the PLSUKF, used the current and the

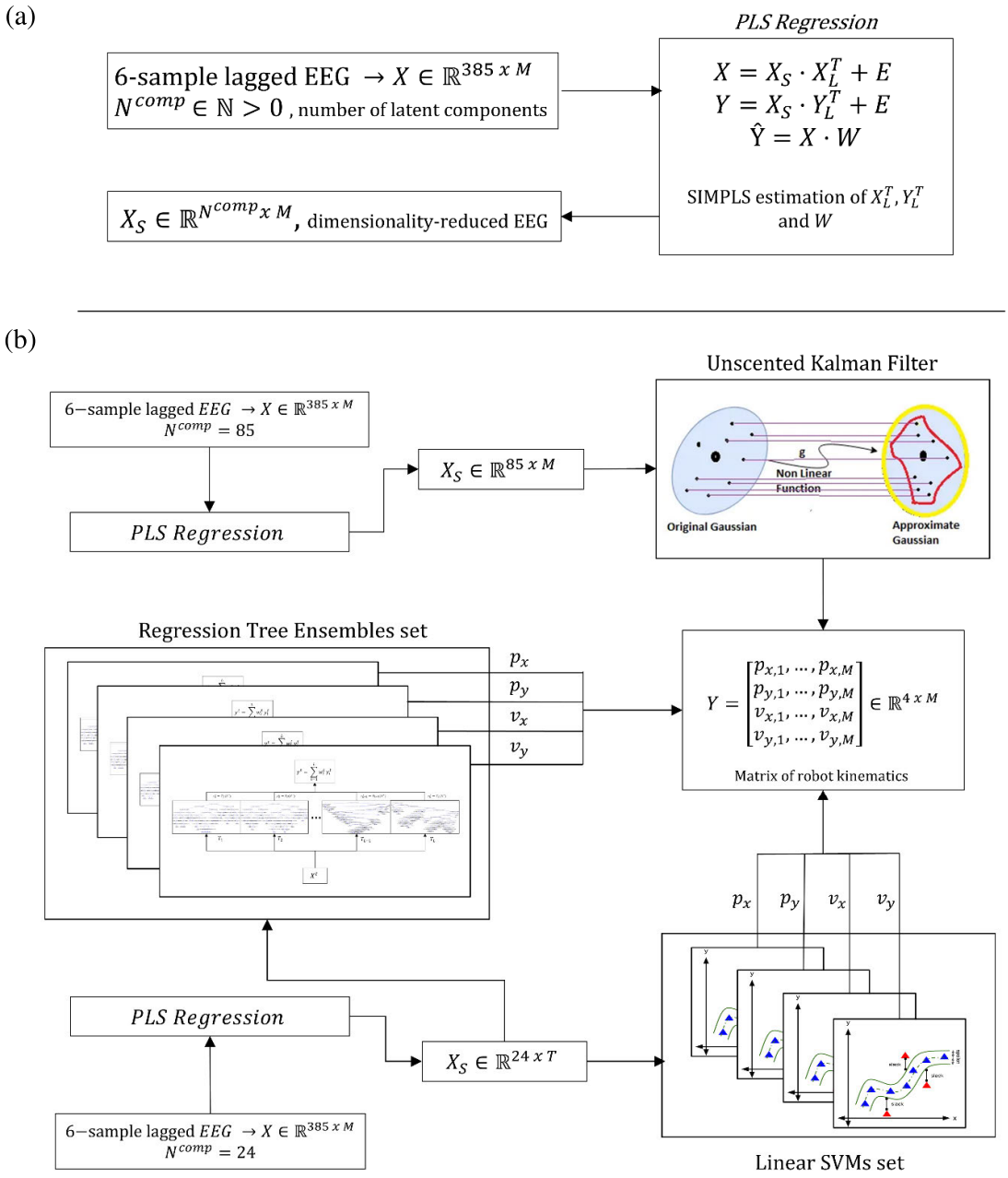

FIGURE 2. Data flow diagram of PLS dimensionality reduction and models -Diagrams representing (a) the Partial Least Squares Regression strategy for input dimensionality reduction and (b) the data flow within the PLSUKF, PLSSVM and PLSRTE models used in the regression task.

preceding 12 lags of the LF-EEG defined in the space of dimensionality $D = 13$ *samples* $\times 55$ *channels* $= 715$.This data were then mapped into a reduced subspace of dimensionality $D_{latent} = 24$. The number of lags and the number of dimensions of the latent space were obtained through cross-validation, as the result of a trade-off between the final decoding performance and the computational load. The successive step involved a set of regularized linear Support Vector Machines (SVM) [43], [44], [45], each trained independently to predict one component of the movement trajectory from the latent-space projected LF-EEG. Formally, given the trajectory component Y_i, the latent-space-transformed EEG X_L, and the linear kernel function $\Phi(\cdot)$, the input-output relationship is defined for the input $w \in X_L$ as:

$$SVM_i = \langle w, \Phi(X_L) \rangle + b = Y_i \quad where$$
$$minimize\ J(w) = \frac{\|w\|}{2}$$
$$subject\ to \begin{cases} Y_i - \langle w, \Phi(X_L) \rangle + b \leq \varepsilon \\ \langle w, \Phi(X_L) \rangle + b - Y_i \geq \varepsilon \end{cases}$$

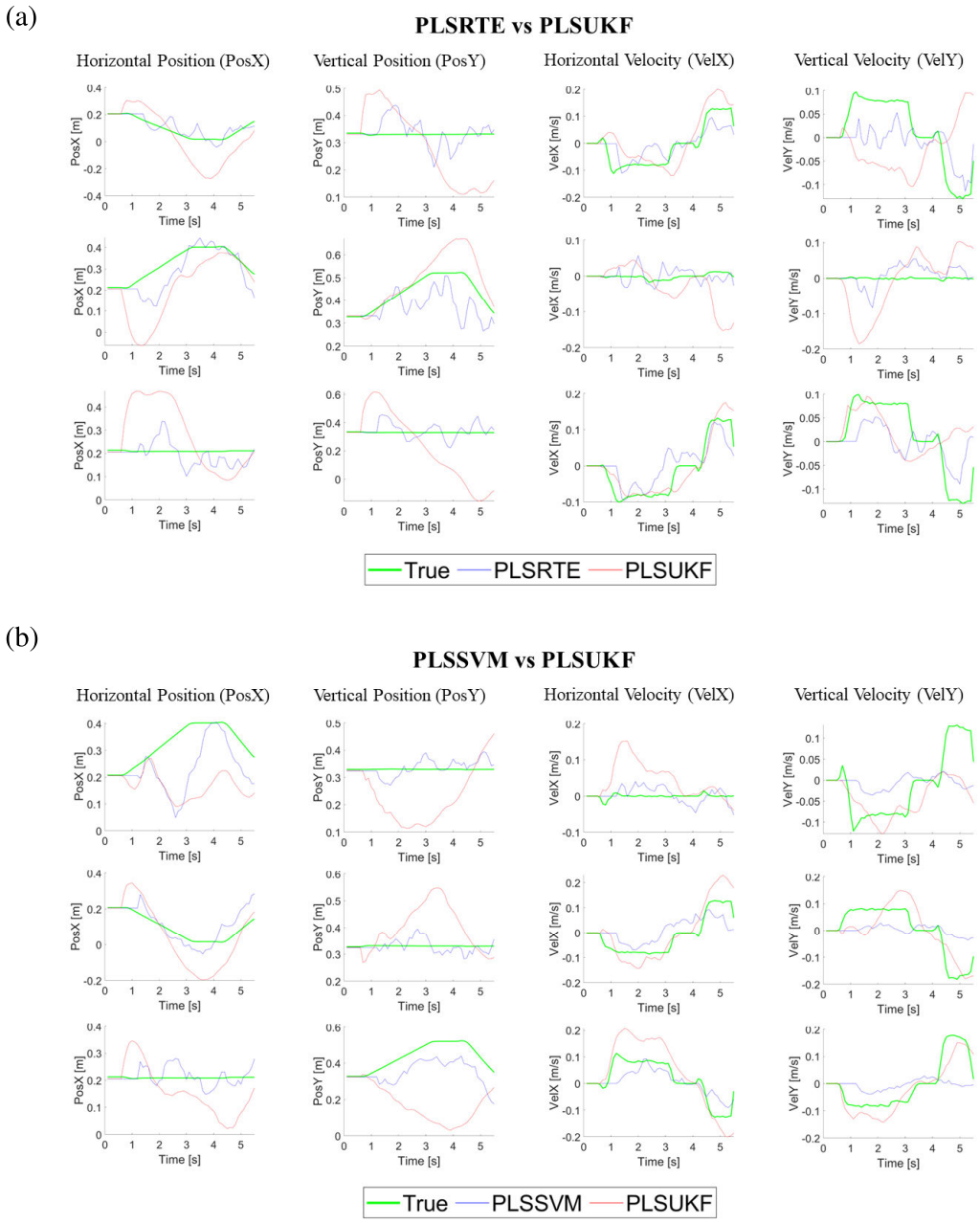

FIGURE 3. Qualitative evaluation of the regression of kinematic parameters from the LF-EEG -Trajectories predicted by (a) PLSSVM (blue lines) and PLSUKF (red lines) and (b) PLSRTE (blue lines) and PLSUKF (red lines) compared to the true ones (green lines). For each movement parameter (columns: PosX, PosY, VelX, VelY), each row illustrates a representative example from the best performing subject. t = 0s denotes the start of the trial, t = 0.5 s is the beginning of the reaching movement, t = 3 s is the arrival on the target and t = 4 s is the beginning of the return movement.

The PLSRTE was designed similarly to the PLSSVM model, but the linear SVMs were replaced by an ensemble of regression trees (RTEs). The ensembles' hyper-parameters were selected through grid-search optimization with cross-validation [46], [47], [48]. Each ensemble was composed of 400 weak learners, i.e., binary regression trees of depth d = 100, fitted using the Least-Squares Boosting algorithm [46], [48], and the final prediction of the model was defined as the weighted average of the weak learners' predictions, smoothed by a 3-samples wide moving average across the temporal dimension of the output.

Within each subject, trials were randomly split into 80 % training – 20 % testing stratified partitions. The chosen model was trained and fine-tuned on 80% of trials and tested and evaluated on the remaining 20%. Hyperparameter optimization was achieved through grid search using 5-fold cross-validation on the training set. For each participant, all

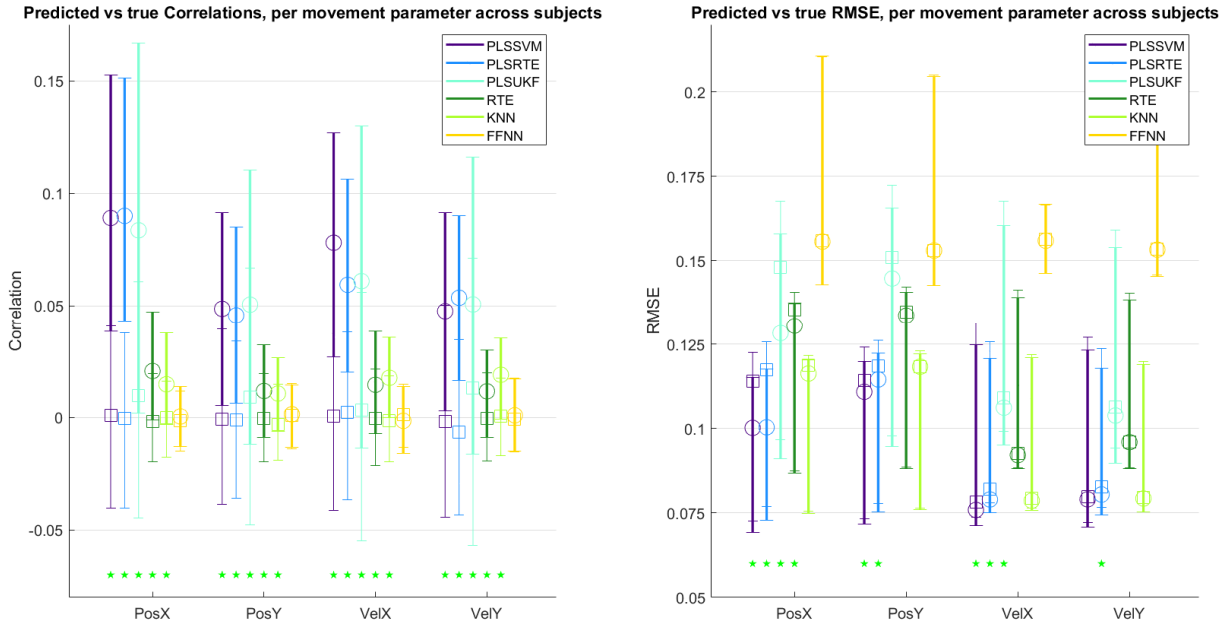

FIGURE 4. Pearson's correlation coefficient (left) and RMSE (right) results -Across-subject distributions of each model, correlation (right) and RMSE (left) are displayed for each movement parameter. Within each condition and model, green stars mark significantly ($p < 0.001$) above chance-level prediction performance, i.e., between the thick-lined distribution (circle-marker median) and the thin-lined chance-level distribution (square-marker median). The models included in this analysis are PLSSVM, PLSRTE, PLSUKF, standard Regression Tree Ensemble, KNN Regression and 2-layers feedforward Neural Network.

the EEG trials in the testing sets were randomly shuffled for 50 iterations, and the model's predictions were evaluated on each shuffling iteration. The performance relative to the shuffled data for each iteration and participant represents the distribution of the chance-level baseline. The test performance and the chance-level performance were evaluated in terms of two selected measures, i.e., the Pearson's Correlation Coefficient r and the Root Mean Square Error RMSE, in line with previous non-invasive and invasive BCI studies [49]. The first captures the linear association between the true and predicted trajectories, and it is computed separately for each kinematic parameter (horizontal and vertical position and velocity) over all testing trials. The second captures the absolute error between the true and predicted trajectories and it is calculated, for each type of parameter, as the square root of the time-averaged squared difference between the predicted and the true trajectories over all testing trials. The process was repeated for each of the six models: PLSSVM, PLSRTE, PLSUKF, standard RTE (Regression Tree Ensemble with 100 weak learners, depth $d = 5$), k-Nearest Neighbours Regressor (KNN) [50] and a simple 2-layer Feed-forward Neural Network (FFNN, one fully-connected layer from the 55-features EEG sample vector to 50 hidden units, then 0.125 dropout and a fully-connected regression layer to the 4 output dimension of the kinematic trajectories).

III. RESULTS

A. CONTINUOUS DECODING

We compared the predicted trajectories with the true trajectories using all the methods described. Figures 3(a) and 3(b) depict the true and predicted trajectories (horizontal and vertical position and velocity) based on PLSUKF, PLSSVM and PLSRTE from representative trials of the best-performing subject. In Figure 4 we present the resulting average (over all trials) correlation coefficient (left panel) and RMSE (right panel) distribution along with its median (empty circle) and its span between the 25th and 75th percentiles (vertical line) across all participants. The distributions were computed comparing the predicted and true kinematic trajectories of PLSRTE, PLSSVM, PLSUKF, KNN, classic RTE and feed-forward neural network (NN), and were assessed for non-Gaussianity using a Lilliefors test. The distributions of the chance-level results are visually represented by means of their span between the 25th and 75th percentiles (vertical thin line) and their median (empty square). Green stars mark significantly above chance-level prediction performance ($p < 0.001$). To evaluate the presence of significant differences between algorithms, we applied a Kruskal Wallis test corrected for multiple comparisons using the Benjamini & Yekutieli method [51]. The test was applied to the distributions of each performance measure for each model, independently for each kinematic parameter. The

TABLE 1. Median ± 95% confidence interval of the Pearson's Correlation coefficient *r* between the true trajectories and the predicted ones based on the PLSUKF, PLSSVM and PLSRTE models, for each kinematic parameter, averaged across subjects. The chance level was obtained through the same procedure but shuffling the input data trial-wise before the computation of the correlation.

r	Position X	Position Y	Velocity X	Velocity Y
PLSUKF	0.128 ± 0.033	0.145 ± 0.036	0.106 ± 0.033	0.104 ± 0.032
PLSUKF chance	0.148 ± 0.035	0.151 ± 0.037	0.109 ± 0.034	0.107 ± 0.032
PLSSVM	0.1 ± 0.023	0.111 ± 0.024	0.076 ± 0.027	0.079 ± 0.026
PLSSVM chance	0.114 ± 0.025	0.114 ± 0.025	0.078 ± 0.029	0.08 ± 0.027
PLSRTE	0.1 ± 0.023	0.115 ± 0.024	0.079 ± 0.023	0.081 ± 0.022
PLSRTE chance	0.117 ± 0.024	0.119 ± 0.024	0.082 ± 0.024	0.083 ± 0.024

TABLE 2. Median ± 95% confidence interval of the RMSE between the true trajectories and the predicted ones based on the PLSUKF, PLSSVM and PLSRTE models, for each kinematic parameter, averaged across subjects. The chance level was obtained through the same procedure but shuffling the input data trial-wise before the computation of the RMSE.

RMSE	Position X	Position Y	Velocity X	Velocity Y
PLSUKF	0.084 ± 0.082	0.051 ± 0.061	0.061 ± 0.072	0.051 ± 0.066
PLSUKF chance	0.01 ± 0.053	0.01 ± 0.057	0.003 ± 0.055	0.013 ± 0.064
PLSSVM	0.089 ± 0.057	0.049 ± 0.043	0.078 ± 0.05	0.048 ± 0.044
PLSSVM chance	0.001 ± 0.041	0.001 ± 0.039	0.001 ± 0.042	-0.002 ± 0.047
PLSRTE	0.09 ± 0.054	0.046 ± 0.039	0.059 ± 0.043	0.054 ± 0.037
PLSRTE chance	0.001 ± 0.039	-0.001 ± 0.035	0.002 ± 0.037	-0.007 ± 0.039

test's results are displayed in Figure S1 of the Supplementary material.

The RMSE/correlation results are reported in Tables 1 and 2, averaged over subjects and iterations, for the PLSSVM, PLSRTE and PLSUKF.

B. CHANNEL CONTRIBUTION TO THE CONTINUOUS DECODING PERFORMANCE

The removal of the anterio-frontal channels for the kinematics regression was motivated by the hypothesis that oculomotor activity might be affecting the decoding performance. In order to validate this hypothesis, each channel's contribution was estimated by retraining a PLSRTE model using all EEG channels including the AF channels. The contribution of a channel to the final decoding performance was quantified by measuring the change in testing correlation/RMSE values when that particular channel was excluded from the model. The main concept behind this approach is that if a channel's information significantly impacts the decoding performance, omitting it will lead to correlation/RMSE changes, underlining its importance in the model. The results of this analysis are shown in Figure 5, where topographical plots display, for each channel, the absolute difference between the correlation (Fig. 5a) and RMSE (Fig. 5b) obtained by omitting that channel and the ones obtained using all channels. We observed a large contribution of the AF channels to the decoding performance, affirming our approach of excluding these channels for the decoding analysis.

In Fig. 5c and Fig. 5d, we repeated the same procedure but this time, we omitted the AF channels from the analysis. Each channel's contribution was estimated by retraining a PLSRTE model using all EEG channels except the AF channels. The assessment of a channel's contribution to the final decoding performance involved quantifying the change in testing correlation/RMSE values upon excluding that specific channel from the model. By excluding the AF channels, the contribution of previously overshadowed channels, associated with visual processing and motor-related information in the centro-parietal and parieto-occipital regions became more prominent.

C. ERD/S ANALYSIS

Additionally to the decoding analysis, we extracted topographical maps of ERD/S in the α/μ (8-12 Hz) and β(12-30 Hz) bands, to determine the neurophysiological effects of the observation of robotic movements. Figure 6 illustrates the average (over all subjects) time evolution of the ERD/S maps within a trial. The activity elicited by the observation of the movement typically emerges 0.5 s after movement initiation, generally located in the centro-parietal and parieto-occipital regions.

ERD/S was further calculated for each participant in restriction to the target of the observed movement, i.e., for each target i (for i=1…8, as defined in Figure 1(b)), an ERD/S map was obtained from trials in which the movement was directed exclusively toward that target, e.g., ERD/S1 was obtained from trials associated with movements toward the upper-left target, labelled as "1". The ERD/S directional difference was then computed by subtracting the synchronization level associated to opposite targets along a direction, that is:

$$\begin{aligned}\Delta ERD/S_{horizontal} &= ERD/S_1 + ERD/S_2 + ERD/S_3 \\ &\quad - (ERD/S_6 + ERD/S_7 + ERD/S_8)\end{aligned} \tag{2}$$

$$\begin{aligned}\Delta ERD/S_{vertical} &= ERD/S_1 + ERD/S_4 + ERD/S_6 \\ &\quad - (ERD/S_3 + ERD/S_5 + ERD/S_8)\end{aligned}$$

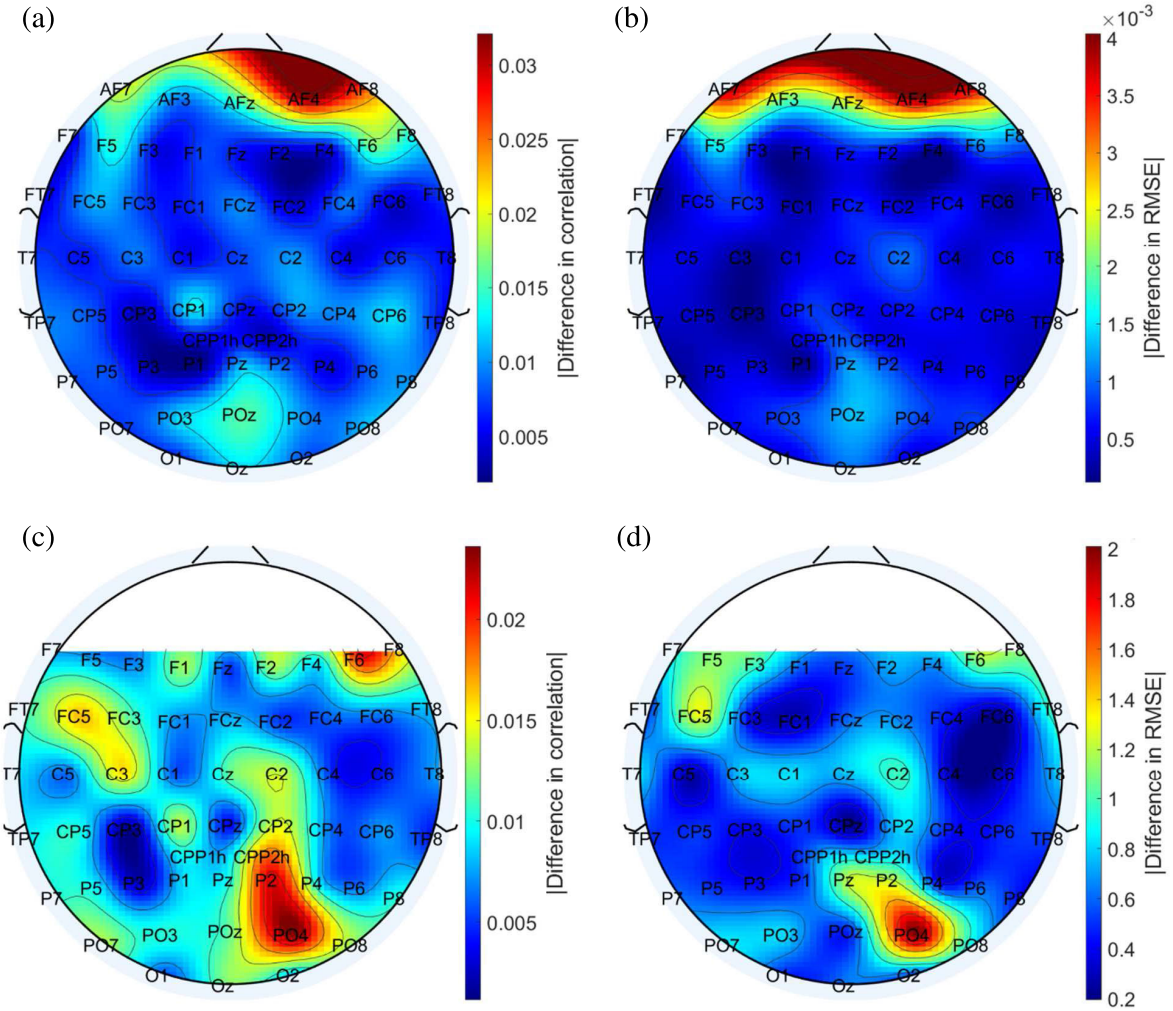

FIGURE 5. Topographical maps of each channel's contribution to the decoding performance -The topographical maps illustrate the changes in (a) correlation and (b) RMSE values resulting from excluding a channel from the PLSRTE model, comparing it to the full model that includes all channels. Specifically, for each channel C, we trained a PLSRTE kinematics decoder on all EEG channels except C and measured the absolute difference in correlation and RMSE compared to the model trained on all EEG channels. Results show that the largest performance drop is obtained when removing AFs channels, highlighting the informational content of these channels in the decoding process. Our hypothesis is that the presence of artifact residuals overshadow, at informational level, channels related to motor and visual processing. This motivates our choice of removing AF lines in the actual decoding process.
Maps (c) and (d) are obtained similarly as in (a) and (b) but excluding the AF lines activity from the analysis. These results have the purpose of validating the effectiveness of the removal of AF lines. Indeed, the most significant chances in performance are now registered when excluding channels in central to occipital areas, notoriously associated to the neural processes of interest.

It should be mentioned that the return movement had an opposite direction to the one induced by the trial's target position, since the movement progresses from the target towards the central position. For example, within a trial, a reaching movement towards a target on the left corresponds to a return movement towards the right.

The temporal progression of such quantities was inspected, and intervals of interest were selected specifically for each direction. The differences of each participant were then averaged within those intervals. Moreover, in order to assess statistically significant differences between ROIs in the directional specificity of ERD/S, electrodes were divided in six regions of interest (ROIs) — fronto-central left, fronto-central right, centro-parietal left, centro-parietal right, parieto-occipital left and parieto-occipital right. The ERD difference in each interval was averaged within each ROI, and one-way ANOVA tests corrected for multiple comparisons (using the Benjamini-Hochberg method [52]) were performed between the resulting distributions of spatially- and temporally averaged ERD/S differences. The resulting topographical maps are displayed in Figure 7, with different dashed lines marking the significance level of Δ ERD/S between ROIs. Relevant features for the horizontal difference include stronger desynchronization in the right parieto-occipital region for rightmost targets during the preparation phase, in the centro-parietal and parieto-occipital

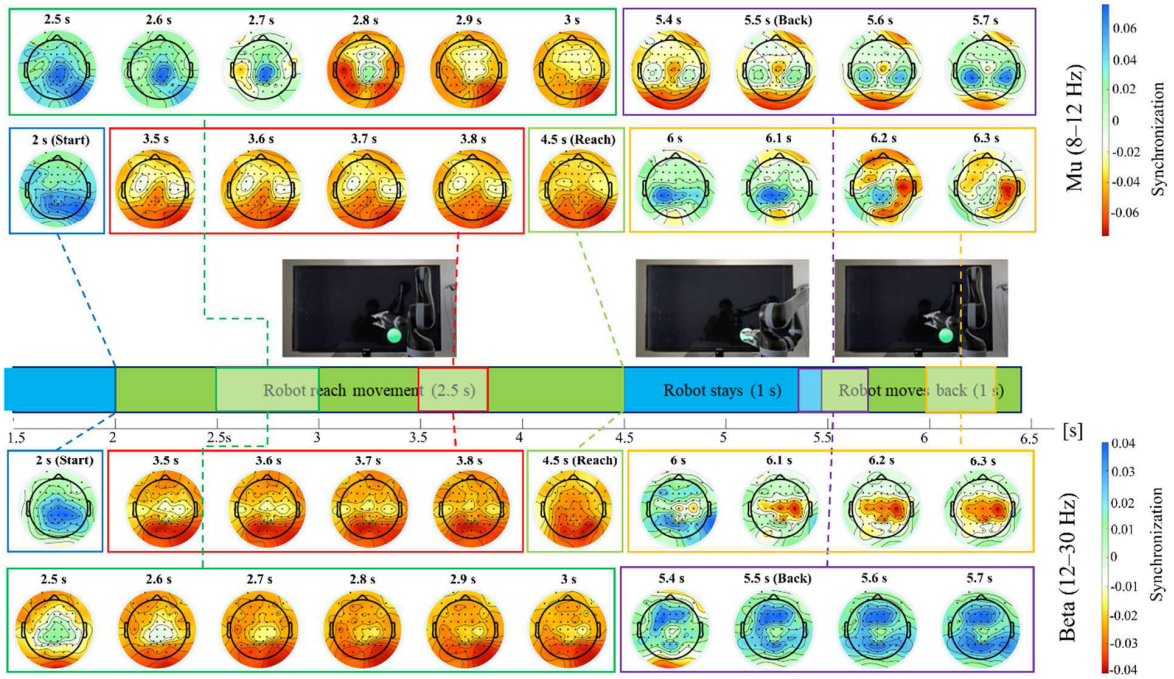

FIGURE 6. Topographic maps of ERD/S in the mu and beta band - averaged over all subjects. Intervals and time points of reference within the trial are indicated by the color-coded blocks. The middle panel depicts a schematization of the trial's phases in time.

region contralaterally to the movement direction around the reaching movement onset, and ipsilaterally in the same regions during the movement's progression toward the target. Regarding the vertical difference, uppermost targets were observed to induce direction-specific ERD/S similarly to the leftmost targets in the horizontal case, and analogously lowermost targets showed similar effects to the ones of rightmost targets in the horizontal case.

IV. DISCUSSION

In this study, we gathered data on human movement observation, analysed it in terms of well-known motor-related spectral features and employed it to reconstruct the movement of a robotic arm. Our goal was to demonstrate the feasibility of observation-based calibration with EEG. While invasive brain measurements of movement observation have been shown to provide satisfactory results [13], [14], the practice of measuring neural activity at the scalp level instead of using electrodes implanted into cortical tissues carries well-known challenges that affect the interpretation and decoding of EEG signals. One of these challenges resides in the unavoidable link between movement observation tasks and artifacts of oculomotor activity in EEG, since it is not possible to restrict the gaze to a specific point as often done in ME, MA and MI tasks. Therefore, the removal of visual artifacts and overt eye movements from the EEG has been a crucial step in this study. Such artifacts were observed to affect a number of channels, mostly the AF electrodes. Consequently, these channels were excluded during the pre-processing stage. The results of the channel contribution analysis at Figure 5 highlight an overshadowing effect exerted by the AF electrodes — the ones with the highest contribution — on channels carrying actual motor-related content. This underscores the necessity of excluding AF channels during the pre-processing phase.

As can be observed from the qualitative evaluation in Figure 3 the PLSUKF prediction displays undershooting and amplitude mismatch when compared to the true trajectories, possibly due to the recursive property of the PLSUKF that makes it more suitable for predicting smooth trajectories rather than the jittery or rapidly-shifting trajectories of this task. The PLSSVM was designed in the attempt to address these issues: this solution makes use of double the time lags, mapped in an almost four times smaller subspace compared to the PLSUKF, then decoded into the movement parameters through a set of regularized linear SVM models. The resulting PLSSVM trajectories are visibly more jittery but closer in magnitude and approximately follow the true ones.

The PLSRTE model, on the other hand, was selected to introduce non-linearity in the decoding component by exploiting the RTE model, obtaining results not far from the PLSSVM. It was interesting to observe that the SVM and RTE algorithms, independently utilized without applying PLS, all led to poor decoding performances under the same conditions, suggesting that the combination of the dimensionality reduction effect of the PLS and the predictive capabilities of SVM and RTE are complementary and both necessary to obtain a satisfying decoding performance. The correlation and RMSE results (Figure 4 and Tables 1 and 2)

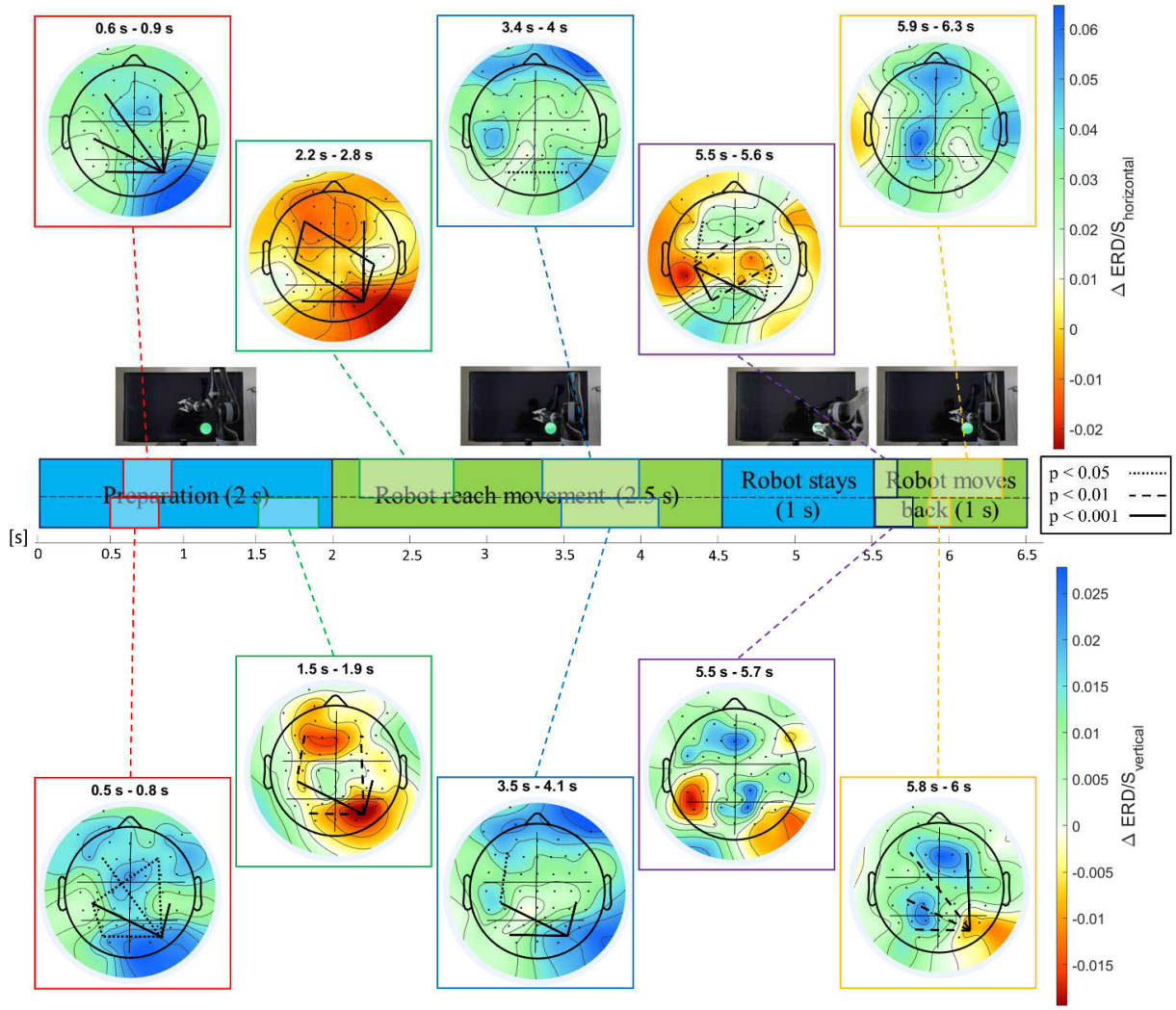

FIGURE 7. ERD/S directional difference along the horizontal (above) and vertical (below) direction - The temporal progression of the trials is displayed in the middle, along with the intervals linked to the respective maps. Negative values of difference in the upper maps mark a desynchronization specific to left targets, and positive values indicate desynchronization for the right targets. For the maps displayed in the bottom, a negative difference signifies patterns specific to the uppermost targets, whereas a positive difference indicates patterns specific to the lowermost targets. In each map, thin black lines display the partitioning of electrodes into ROIs where the one-way ANOVA tests were performed. Thick black lines between ROIs mark a statistically significant difference, with the style of the dashed lines indicating the level of significance.

align with the expectations of high-variance and relatively poor range of values, coherent with the results of similar studies involving MI and ME tasks [9], [14], [29], [37], [40], [41]. Nevertheless, they show that for the PLSRTE, the extraction of motor-related information was indeed successful, leading to a significantly ($p < 0.001$) above-chance correlation and RMSE in all conditions considered. For the PLSSVM, only 12.5% of the conditions was not significantly above chance, whereas this quantity increases to 25% in the case of the PLSUKF, 50% in the case of RTE and KNN, and up to 100% for the feed-forward NN. Furthermore, the significance tests between models (Supplementary material, Figure S1) show that in terms of correlation, PLSSVM, PLSRTE and PLSUKF all significantly ($p < 0.001$) outperformed the standard RTE, KNN and NN, with the novel models performing better than the PLSUKF only in the PosX condition. In terms of RMSE, the PLSSVM, PLSRTE and KNN all performed significantly better than PLSUKF, RTE and NN. Through the novel models it was possible to reduce the RMSE of the PLSUKF in 62.5% of cases, contributing to an average decrease of the distribution's median by 23.5%.

To further support our results in the regression task, in [53] we carried out a classification task where we predicted the target of the observed movement from multiple time windows of the LF-EEG recorded during motor observation, with promising results. However, since the models and algorithms used in the classification are not directly comparable to the regression analysis presented here, we have chosen not to include it in this work.

In terms of the ERD/S analysis, α/μ and β band ERD/S maps exhibited similar patterns, with suppression starting simultaneously with the initiation of the movement in the rightmost parieto-occipital cortex, ERS arising bilaterally in the central line during the target-directed movement, and difference analysis was carried out to investigate characteristics of the observational neural activity in the alpha band related to the direction of the observed movement (Figure 7). Along the horizontal direction, i.e., comparing ERD/S patterns during the observation of left-directed movements with the ones of right-directed movements, significant differences were found: 1) during the preparation of the movement ipsilaterally to the cued side, attributed to the phenomenon of covert visuospatial attention (CVSA) [54], [55]; 2) at the onset of both the reaching and the going-back movements in the centro-parietal and parieto-occipital regions; and, 3) during the target-approach phase of both movements, ipsilaterally to the target's side in the parieto-occipital region. In the vertical case a similar specificity of ERD emerging in the vicinity of C4 during the rapid return movement to the home position. Additionally, a directional pattern was found, with the uppermost and lowermost targets behaving similarly to leftmost and rightmost respectively, despite a generally lower difference amplitude.

V. LIMITATIONS OF THE STUDY

A major issue that affected this study was the scarcity of data and the limited computational capabilities. With an average of 230 trials per subject, translating into 1495 seconds (25 minutes, 12650 samples) per subject for training and testing, the development of more sophisticated models and deep learning-based techniques was severely hindered. Additionally, this resulted in the need of evaluating several reiterations of the training-and-testing procedure to avoid overfitting and to obtain statistically reliable results, further restricting the choice of the decoding algorithms to simpler models with low training time.

The limited amount of recorded data was a direct consequence of the complexity of the setup, which involved the repetition of an observational task several times in the span of hours. Longer durations would have affected the level of attention and tiredness of the participants. Therefore, refining the paradigm and the experimental setup could allow for the collection of a larger amount of data. Consequently, this could expand the range of possible techniques and possibly enhance decoding performance.

Despite these obstacles, this study succeeds in the purpose of demonstrating the transferability of observation-based calibration from invasive to non-invasive BCI systems.

VI. FUTURE DIRECTIONS

The results highlight the value of observation-based calibration procedures for training non-invasive BCIs in motor command regression, supporting their inclusion in future studies in this field and potentially in the learning pipeline for closed-loop neuroprosthetic control. Moreover, they demonstrate the feasibility of reconstructing robotic movements from their neural encoding, although they are limited by the issues discussed in the previous section. In this context, further studies could focus on overcoming these limitations, for example through the inclusion of more advanced and complex algorithms and techniques, such as deep learning and transfer learning. Furthermore, we introduced two new models for the regression of kinematic trajectories from EEG. Their promising results, compared to other similar models, require further validation through additional studies, whether in the same context as this study or in other regression tasks. This will help establish them as part of the broader category of machine learning models for EEG regression.

VII. CONCLUSION

In this study, we examined how neural activity, captured through non-invasive EEG, encodes the observation of robotic movements described by specific characteristics, such as center-out and target-directed translations. Our research introduces the possibility of exploring observation-based calibration using non-invasive EEG data alongside novel techniques, and simultaneously paves the way towards the implementation of a closed-loop control framework.

ETHICAL STATEMENT

All participants gave their written informed consent to take part in the study, and the experimental procedure conformed to the Declaration of Helsinki and was approved by the ethics committee of the Medical University of Graz.

CONFLICT OF INTEREST

The authors declare that the research was conducted in the absence of any commercial or financial relationships that could be construed as a potential conflict of interest.

AUTHOR CONTRIBUTIONS

Gernot Müller-Putz conceived the experiment. Pietro Cimarosto and Gernot Müller-Putz designed the experiment and the paradigm. Pietro Cimarosto performed the experiment. Pietro Cimarosto processed and analyzed the data. Kyriaki Kostoglou, Gernot Müller-Putz, and Luca Tonin supervised the analyses and proofread the manuscript. Pietro Cimarosto wrote the manuscript, Kyriaki Kostoglou, Gernot Müller-Putz, and Luca Tonin reviewed the manuscript. All authors contributed to the article and approved the submitted version.

ACKNOWLEDGMENT

The dataset and code of the experiment will be made available upon reasonable request.

REFERENCES

[1] J. R. Wolpaw, J. del R. Millán, and N. F. Ramsey, "Brain-computer interfaces: Definitions and principles," in *Handbook of Clinical Neurology*, vol. 168, N. F. Ramsey and J. del R. Millán, Eds., Amsterdam, The Netherlands: Elsevier, 2020, ch. 2, pp. 15–23, doi: 10.1016/B978-0-444-63934-9.00002-0.

[2] G. R. Müller-Putz, "Electroencephalography," in *Handbook of Clinical Neurology*, vol. 168, N. F. Ramsey and J. del R. Millán, Eds., Amsterdam, The Netherlands: Elsevier, 2020, ch. 1, pp. 249–262, doi: 10.1016/B978-0-444-63934-9.00018-4.

[3] R. Scherer, F. Lee, A. Schlogl, R. Leeb, H. Bischof, and G. Pfurtscheller, "Toward self-paced brain–computer communication: Navigation through virtual worlds," *IEEE Trans. Biomed. Eng.*, vol. 55, no. 2, pp. 675–682, Feb. 2008, doi: 10.1109/TBME.2007.903709.

[4] S. Tortora, A. Gottardi, E. Menegatti, and L. Tonin, "Continuous teleoperation of a robotic manipulator via brain-machine interface with shared control," in *Proc. IEEE 27th Int. Conf. Emerg. Technol. Factory Autom. (ETFA)*, Sep. 2022, pp. 1–8, doi: 10.1109/ETFA52439.2022.9921526.

[5] B. Obermaier, G. R. Müller, and G. Pfurtscheller, "'Virtual keyboard' controlled by spontaneous EEG activity," *IEEE Trans. Neural Syst. Rehabil. Eng.*, vol. 11, no. 4, pp. 422–426, Dec. 2003, doi: 10.1109/TNSRE.2003.816866.

[6] G. Pfurtscheller, C. Neuper, G. R. Müller, B. Obermaier, G. Krausz, A. Schlogl, R. Scherer, B. Graimann, C. Keinrath, D. Skliris, M. Wortz, G. Supp, and C. Schrank, "Graz-BCI: State of the art and clinical applications," *IEEE Trans. Neural Syst. Rehabil. Eng.*, vol. 11, no. 2, pp. 1–4, Jun. 2003, doi: 10.1109/TNSRE.2003.814454.

[7] T. Kaufmann, S. M. Schulz, C. Grünzinger, and A. Kübler, "Flashing characters with famous faces improves ERP-based brain–computer interface performance," *J. Neural Eng.*, vol. 8, no. 5, Oct. 2011, Art. no. 056016.

[8] A. Kreilinger, H. Hiebel, and G. R. Müller-Putz, "Single versus multiple events error potential detection in a BCI-controlled car game with continuous and discrete feedback," *IEEE Trans. Biomed. Eng.*, vol. 63, no. 3, pp. 519–529, Mar. 2016, doi: 10.1109/TBME.2015.2465866.

[9] H. S. Pulferer, B. Ásgeirsdóttir, V. Mondini, A. I. Sburlea, and G. R. Müller-Putz, "Continuous 2D trajectory decoding from attempted movement: Across-session performance in able-bodied and feasibility in a spinal cord injured participant," *J. Neural Eng.*, vol. 19, no. 3, May 2022, Art. no. 036005, doi: 10.1088/1741-2552/ac689f.

[10] G. Pfurtscheller and F. H. L. da Silva, "Event-related EEG/MEG synchronization and desynchronization: Basic principles," *Clin. Neurophysiol.*, vol. 110, no. 11, pp. 1842–1857, Nov. 1999, doi: 10.1016/s1388-2457(99)00141-8.

[11] S. D. Muthukumaraswamy and B. W. Johnson, "Primary motor cortex activation during action observation revealed by wavelet analysis of the EEG," *Clin. Neurophysiol.*, vol. 115, no. 8, pp. 1760–1766, Aug. 2004, doi: 10.1016/j.clinph.2004.03.004.

[12] S. Rossi, F. Tecchio, P. Pasqualetti, M. Ulivelli, V. Pizzella, G. L. Romani, S. Passero, N. Battistini, and P. M. Rossini, "Somatosensory processing during movement observation in humans," *Clin. Neurophysiol.*, vol. 113, no. 1, pp. 16–24, Jan. 2002, doi: 10.1016/S1388-2457(01)00725-8.

[13] S. T. Clanton, "Brain–computer interface control of an anthropomorphic robotic arm," Doctor thesis, Robot. Inst., Carnegie Mellon Univ., Pittsburgh, PA, USA, 2011, doi: 10.1184/R1/6715016.v1.

[14] J. L. Collinger, B. Wodlinger, J. E. Downey, W. Wang, E. C. Tyler-Kabara, D. J. Weber, A. J. Mcmorland, M. Velliste, M. L. Boninger, and A. B. Schwartz, "High-performance neuroprosthetic control by an individual with tetraplegia," *Lancet*, vol. 381, no. 9866, pp. 557–564, Feb. 2013, doi: 10.1016/S0140-6736(12)61816-9.

[15] H. A. Agashe and J. L. Contreras-Vidal, "Observation-based calibration of brain-machine interfaces for grasping," in *Proc.6th Int. IEEE/EMBS Conf. Neural Eng. (NER)*, Nov. 2013, pp. 1–4, doi: 10.1109/NER.2013.6695856.

[16] K. K. Ang, C. Guan, C. Wang, K. S. Phua, A. H. G. Tan, and Z. Y. Chin, "Calibrating EEG-based motor imagery brain–computer interface from passive movement," in *Proc. Annu. Int. Conf. IEEE Eng. Med. Biol. Soc.*, Aug. 2011, pp. 4199–4202, doi: 10.1109/IEMBS.2011.6091042.

[17] S. Frenkel-Toledo, S. Bentin, A. Perry, D. G. Liebermann, and N. Soroker, "Dynamics of the EEG power in the frequency and spatial domains during observation and execution of manual movements," *Brain Res.*, vol. 1509, pp. 43–57, May 2013, doi: 10.1016/j.brainres.2013.03.004.

[18] D. Ertelt, C. Hemmelmann, C. Dettmers, A. Ziegler, and F. Binkofski, "Observation and execution of upper-limb movements as a tool for rehabilitation of motor deficits in paretic stroke patients: Protocol of a randomized clinical trial," *BMC Neurol.*, vol. 12, no. 1, p. 42, Jun. 2012, doi: 10.1186/1471-2377-12-42.

[19] T.-J. Luo, J. Lv, F. Chao, and C. Zhou, "Effect of different movement speed modes on human action observation: An EEG study," *Frontiers Neurosci.*, vol. 12, p. 219, Apr. 2018, doi: 10.3389/fnins.2018.00219.

[20] S. D. Muthukumaraswamy, B. W. Johnson, and N. A. McNair, "Mu rhythm modulation during observation of an object-directed grasp," *Cognit. Brain Res.*, vol. 19, no. 2, pp. 195–201, Apr. 2004, doi: 10.1016/j.cogbrainres.2003.12.001.

[21] J. A. Pineda, "The functional significance of mu rhythms: Translating 'seeing' and 'hearing' into 'doing,'" *Brain Res. Rev.*, vol. 50, no. 1, pp. 57–68, Dec. 2005, doi: 10.1016/j.brainresrev.2005.04.005.

[22] P. Avanzini, M. Fabbri-Destro, R. D. Volta, E. Daprati, G. Rizzolatti, and G. Cantalupo, "The dynamics of sensorimotor cortical oscillations during the observation of hand movements: An EEG study," *PLoS ONE*, vol. 7, no. 5, May 2012, Art. no. e37534, doi: 10.1371/journal.pone.0037534.

[23] G. Buccino, F. Binkofski, G. R. Fink, L. Fadiga, L. Fogassi, V. Gallese, R. J. Seitz, K. Zilles, G. Rizzolatti, and H.-J. Freund, "Action observation activates premotor and parietal areas in a somatotopic manner: An fMRI study," *Eur. J. Neurosci.*, vol. 13, no. 2, pp. 400–404, Jan. 2001, doi: 10.1111/j.1460-9568.2001.01385.x.

[24] R. Chaisaen, P. Autthasan, N. Mingchinda, P. Leelaarporn, N. Kunaseth, S. Tammajarung, P. Manoonpong, S. C. Mukhopadhyay, and T. Wilaiprasitporn, "Decoding EEG rhythms during action observation, motor imagery, and execution for standing and sitting," *IEEE Sensors J.*, vol. 20, no. 22, pp. 13776–13786, Nov. 2020, doi: 10.1109/JSEN.2020.3005968.

[25] C. Babiloni, F. Babiloni, F. Carducci, F. Cincotti, G. Cocozza, C. Del Percio, D. V. Moretti, and P. M. Rossini, "Human cortical electroencephalography (EEG) rhythms during the observation of simple aimless movements: A high-resolution EEG study," *NeuroImage*, vol. 17, no. 2, pp. 559–572, Oct. 2002, doi: 10.1006/nimg.2002.1192.

[26] S. Cochin, C. Barthelemy, S. Roux, and J. Martineau, "Observation and execution of movement: Similarities demonstrated by quantified electroencephalography," *Eur. J. Neurosci.*, vol. 11, no. 5, pp. 1839–1842, May 1999, doi: 10.1046/j.1460-9568.1999.00598.x.

[27] R. Gatti, A. Tettamanti, P. M. Gough, E. Riboldi, L. Marinoni, and G. Buccino, "Action observation versus motor imagery in learning a complex motor task: A short review of literature and a kinematics study," *Neurosci. Lett.*, vol. 540, pp. 37–42, Apr. 2013, doi: 10.1016/j.neulet.2012.11.039.

[28] T. J. Bradberry, R. J. Gentili, and J. L. Contreras-Vidal, "Reconstructing three-dimensional hand movements from noninvasive electroencephalographic signals," *J. Neurosci.*, vol. 30, no. 9, pp. 3432–3437, Mar. 2010, doi: 10.1523/jneurosci.6107-09.2010.

[29] P. Ofner and G. R. Müller-Putz, "Decoding of velocities and positions of 3D arm movement from EEG," in *Proc. Annu. Int. Conf. IEEE Eng. Med. Biol. Soc.*, Aug. 2012, pp. 6406–6409, doi: 10.1109/EMBC.2012.6347460.

[30] H. S. Pulferer, B. Ásgeirsdóttir, V. Mondini, A. I. Sburlea, and G. Müller-Putz, "Learning effects in 2D trajectory inference from low-frequency EEG signals over multiple feedback sessions," in *Proc. Annu. Meeting Austrian Soc. Biomed. Eng.*, Jun. 2021, pp. 83–86, doi: 10.3217/978-3-85125-826-4-22.

[31] V. Mondini, A.-I. Sburlea, and G. R. Müller-Putz, "Towards unlocking motor control in spinal cord injured by applying an online EEG-based framework to decode motor intention, trajectory and error processing," *Sci. Rep.*, vol. 14, no. 1, p. 4714, Feb. 2024, doi: 10.1038/s41598-024-55413-x.

[32] G. R. Müller-Putz, R. J. Kobler, J. Pereira, C. Lopes-Dias, L. Hehenberger, V. Mondini, V. Martínez-Cagigal, N. Srisrisawang, H. Pulferer, L. Batistić, and A. I. Sburlea, "Feel your reach: An EEG-based framework to continuously detect goal-directed movements and error processing to gate kinesthetic feedback informed artificial arm control," *Frontiers Hum. Neurosci.*, vol. 16, Mar. 2022, Art. no. 841312, doi: 10.3389/fnhum.2022.841312.

[33] J. Pereira, R. Kobler, P. Ofner, A. Schwarz, and G. R. Müller-Putz, "Online detection of movement during natural and self-initiated reach-and-grasp actions from EEG signals," *J. Neural Eng.*, vol. 18, no. 4, Aug. 2021, Art. no. 046095, doi: 10.1088/1741-2552/ac0b52.

[34] J. Pereira, P. Ofner, A. Schwarz, A. I. Sburlea, and G. R. Müller-Putz, "EEG neural correlates of goal-directed movement intention," *NeuroImage*, vol. 149, pp. 129–140, Apr. 2017, doi: 10.1016/j.neuroimage.2017.01.030.

[35] R. J. Kobler, A. I. Sburlea, C. Lopes-Dias, A. Schwarz, M. Hirata, and G. R. Müller-Putz, "Corneo-retinal-dipole and eyelid-related eye artifacts can be corrected offline and online in electroencephalographic and magnetoencephalographic signals," *NeuroImage*, vol. 218, Sep. 2020, Art. no. 117000, doi: 10.1016/j.neuroimage.2020.117000.

[36] R. J. Kobler, A. I. Sburlea, and G. R. Müller-Putz, "A comparison of ocular artifact removal methods for block design based electroencephalography experiments," in *Proc. GBCIC*, 2017, pp. 1–6.

[37] V. Mondini, R. J. Kobler, A. I. Sburlea, and G. R. Müller-Putz, "Continuous low-frequency EEG decoding of arm movement for closed-loop, natural control of a robotic arm," *J. Neural Eng.*, vol. 17, no. 4, Aug. 2020, Art. no. 046031, doi: 10.1088/1741-2552/aba6f7.

[38] R. J. Kobler, A. I. Sburlea, V. Mondini, and G. R. Müller-Putz, "HEAR to remove pops and drifts: The high-variance electrode artifact removal (HEAR) algorithm," 2019, *arXiv:1907.12354*.

[39] B. Graimann, B. Z. Allison, and G. Pfurtscheller, *Brain-Computer Interfaces: Revolutionizing Human–Computer Interaction* (The Frontiers Collection). Heidelberg, Germany: Springer, 2011. [Online]. Available: https://books.google.it/books?id=PeoEvgAACAAJ

[40] R. J. Kobler, A. I. Sburlea, V. Mondini, M. Hirata, and G. R. Müller-Putz, "Distance- and speed-informed kinematics decoding improves M/EEG based upper-limb movement decoder accuracy," *J. Neural Eng.*, vol. 17, no. 5, Nov. 2020, Art. no. 056027, doi: 10.1088/1741-2552/abb3b3.

[41] D. Borra, V. Mondini, E. Magosso, and G. R. Müller-Putz, "Decoding movement kinematics from EEG using an interpretable convolutional neural network," *Comput. Biol. Med.*, vol. 165, Oct. 2023, Art. no. 107323, doi: 10.1016/j.compbiomed.2023.107323.

[42] R. E. Kalman, "A new approach to linear filtering and prediction problems," *J. Basic Eng.*, vol. 82, no. 1, pp. 35–45, Mar. 1960, doi: 10.1115/1.3662552.

[43] V. N. Vapnik, *The Nature of Statistical Learning Theory*. New York, NY, USA: Springer, 1995.

[44] F. Lotte, L. Bougrain, A. Cichocki, M. Clerc, M. Congedo, A. Rakotomamonjy, and F. Yger, "A review of classification algorithms for EEG-based brain–computer interfaces: A 10 year update," *J. Neural Eng.*, vol. 15, no. 3, Jun. 2018, Art. no. 031005, doi: 10.1088/1741-2552/aab2f2.

[45] A. J. Smola and B. Schölkopf, "A tutorial on support vector regression," *Statist. Comput.*, vol. 14, no. 3, pp. 199–222, Aug. 2004.

[46] L. Breiman, "Random forests," *Mach. Learn.*, vol. 45, no. 1, pp. 5–32, 2001, doi: 10.1023/A:1010933404324.

[47] C. Chen and L. Breiman, "Using random forest to learn imbalanced data," Dept. Statist., Univ. California, Berkeley, CA, USA, pp. 1–12, Sep. 2004, vol. 110.

[48] T. G. Dietterich, "Ensemble methods in machine learning," in *Multiple Classifier Systems*. Heidelberg, Germany: Springer, 2000, pp. 1–15.

[49] J. M. Antelis, L. Montesano, A. Ramos-Murguialday, N. Birbaumer, and J. Minguez, "On the usage of linear regression models to reconstruct limb kinematics from low frequency EEG signals," *PLoS ONE*, vol. 8, no. 4, Apr. 2013, Art. no. e61976, doi: 10.1371/journal.pone.0061976.

[50] J. Goldberger, G. E. Hinton, S. Roweis, and R. R. Salakhutdinov, "Neighbourhood components analysis," in *Advances in Neural Information Processing Systems*, L. Saul, Y. Weiss, and L. Bottou, Eds., Cambridge, MA, USA: MIT Press, 2004. [Online]. Available: https://proceedings.neurips.cc/paper_files/paper/2004/file/42fe880812925e520249e808937738d2-Paper.pdf

[51] Y. Benjamini and D. Yekutieli, "The control of the false discovery rate in multiple testing under dependency," *Ann. Statist.*, vol. 29, no. 4, pp. 1165–1188, Aug. 2001, doi: 10.1214/aos/1013699998.

[52] Y. Benjamini and Y. Hochberg, "Controlling the false discovery rate: A practical and powerful approach to multiple testing," *J. Roy. Stat. Society. Ser. B, Methodol.*, vol. 57, no. 1, pp. 289–300, Jan. 1995, doi: 10.1111/j.2517-6161.1995.tb02031.x.

[53] P. Cimarosto, "Decoding and analysis of EEG signals during the motor observation of robotic arm movements," Master thesis, Dept. Inf. Eng., Univ. Padua, Padua, Italy, 2023. Accessed: Oct. 20, 2024. [Online]. Available: https://hdl.handle.net/20.500.12608/48208

[54] L. Tonin, R. Leeb, A. Sobolewski, and J. D. R. Millán, "An online EEG BCI based on covert visuospatial attention in absence of exogenous stimulation," *J. Neural Eng.*, vol. 10, no. 5, Oct. 2013, Art. no. 056007, doi: 10.1088/1741-2560/10/5/056007.

[55] M. S. Worden, J. J. Foxe, N. Wang, and G. V. Simpson, "Anticipatory biasing of visuospatial attention indexed by retinotopically specific α-bank electroencephalography increases over occipital cortex," *J. Neurosci.*, vol. 20, no. 6, p. RC63, Mar. 2000, doi: 10.1523/jneurosci.20-06-j0002.2000.

PIETRO CIMAROSTO received the B.S. degree in information engineering and the M.S. degree in computer engineering from the University of Padua, Italy, in 2023. He developed his master's thesis at the Institute of Neural Engineering, Graz University of Technology, Graz, Austria, on the topics of machine learning for brain computer interfaces and motor observation. His current research interests include passive brain–computer interfaces for spatial attention and workload level detection.

KYRIAKI KOSTOGLOU received the Diploma degree in electrical and computer engineering from the Aristotle University of Thessaloniki (AUTH), Greece, the M.Sc. degree in computer engineering from the University of Cyprus (UCY), Cyprus, and the Ph.D. degree from the Department of Electrical and Computer Engineering, McGill University, Canada, in 2017. The topic of her Ph.D. thesis was the identification of multiple-input time-varying systems and binary response systems for biomedical applications.

She was a Postdoctoral Researcher in medical ultrasound imaging at the Institute of Signal Processing, Johannes Kepler University, Linz, Austria. Currently, she is a Postdoctoral Researcher at the Institute of Neural Engineering, Graz University of Technology, Graz, Austria. Her current research interests include system identification and signal processing for biomedical applications and brain–computer interfaces.

LUCA TONIN (Senior Member, IEEE) received the Ph.D. degree in robotics from École Polytechnique Fédérale de Lausanne (EPFL), Switzerland, in 2013, and the Postdoctoral degree from the Intelligent Autonomous System Laboratory, University of Padua.

From 2016 to 2019, he was a Postdoctoral Researcher at EPFL. He is currently an Associate Professor of computer science at the School of Engineering, University of Padua, Italy. His research is currently focused on exploring advanced techniques for brain–machine interface (BMI)-driven robotics devices. His main contribution to the BMI field is related to the design of novel shared control approaches to improve reliability and enhance the coupling between user and robot. In 2016, he won the first international Cybathlon Paralympic Event as a Co-Leader of the BrainTweakers Team (EPFL). In 2019, he won the Cybathlon BCI Series Paralympic Event as a Leader of the WHI Team (University of Padova). In 2020, his team won the Cybathlon for the third consecutive time.

GERNOT MÜLLER-PUTZ (Senior Member, IEEE) is currently the Head of the Institute of Neural Engineering and the associated Laboratory for Brain–Computer Interfaces, Graz University of Technology, Austria. He has been a Professor of semantic data analysis, since 2014. In his career, he has been a partner or a leader of a number of research projects (EU, ERC), currently, he is a partner of European Innovation Council funded project "INTRECOM." He has published more than 210 peer-reviewed papers with more than 25 800 citations (H-index of 77).

Dr. Müeller-Putz is a founding member of the BCI Society (Treasurer) and the Society for NeuroInformation Systems (NeuroIS.org) and the Deputy Scientific Director. He is a Ludwig-Guttman-Awardee of German Medical Society for Paraplegiology. He is on the board of the Styrian Brain Research Initiative and has been on the board of Austrian Society for Biomedical Engineering, since 2023. He has also been the Dean of the Department of Computer Science and Biomedical Engineering, TU Graz, since October 2023. He is an Associate Editor of IEEE Reviews in Biomedical Engineering and IEEE Transactions in Biomedical Engineering and the Editor-in-Chief of *Frontiers in Human Neuroscience: Brain-Computer Interfaces*.